Current Image Tunneling Spectroscopy of Boron and Nitrogen Co-doped Diamond Films

doi:10.6180/jase.2003.6.3.02

淡江理工學刊, 6(3), 2003

Journal of Applied Science and Engineering, 6(3), 2003

作者/Author： I-Nan Lin;Yi-Ping Chou;Tong T. Chen

頁數/Page： 139-144

出版日期/Publication Date：2003/09

Current Image Tunneling Spectroscopy of Boron and Nitrogen Co-doped Diamond Films

I-Nan Lin[1,2], Yi-Ping Chou[3] and Tong T. Chen[3]

[1] *Department of Physics*
Tamkang University
Tamsui, Taiwan 251, R.O.C.
[2] *Material Science Center*
[3] *Department of Physics*
National Tsing Hua University
Hsinchu, Taiwan 300, R.O.C.
E-mail: inlin@mx.nthu.edu.tw

Abstract

Effect of boron and nitrogen co-doping on the electron field emission properties of the diamond films was examined using current image tunneling spectroscopy in atomic force microscopy (CITS, AFM). Tunneling current-voltage (I_t-V) characteristics measured by AFM indicate that incorporation of boron and nitrogen species induced the presence of impurity state. Such a characteristic is closely related to the local electron field emission behavior of the diamond films. The samples co-doped with 4 sccm boron and 3 sccm nitrogen possess smallest energy gap (E_g = 1.62 eV) and largest emission ratio, as compared with that of other diamond films. These diamond films can be turned on at smallest electric field (E_o = 6.4 V/μm), exhibiting largest field emission capacity (J_e = 1,500 μA/cm^2).

***Key Words*:** Co-doped Diamond Films, Electron Field Emission Properties, Current Image Tunneling Spectroscopy

1. Introduction

Diamond films possess negative electron affinity (NEA) characteristics [1] and are considered to be highly promising for applications in electron field emission devices, such that the related emission properties have been widely investigated [1-3]. Incorporation of dopants into the diamond films to improve their conductivity is necessary for the purpose of enhancing their electron field emission behavior [4-12]. However, the understanding on how the addition of these dopants modifies the materials characteristics and electronic properties of the diamonds is still in primitive stage.

In this paper, the boron and nitrogen species were simultaneously doped into diamond films by biased enhanced nucleation (BEN) in microwave plasma enhanced chemical vapor deposition (MPECVD) process. The influence on the materials characteristics and electronic properties of the boron-doped CVD films was compared with those of the undoped films. Moreover, to understand how the doping of boron doping improves the electron field emission properties of the diamond films, current image tunneling spectroscopic (CITS) technique of atomic force microscopy (AFM) were used to extract the intrinsic parameters related to the electronic structure of the diamond films. The correlation of these parameters with the local electron tunneling behavior of the films was discussed.

2. Experimental

Diamond films were grown by a microwave plasma enhanced chemical vapor deposition process (MPECVD) using ASTex 5400 reactors.

The CH_4/H_2 gases with flow rate of 18 sccm/300 sccm were excited by 2500 W microwave power, where the total pressure in the chamber was maintained at 70 torr. The substrates, which were (100) p-type silicon with 10-50 Ω·cm resistivity, were maintained at around 1000 °C during the growth of diamond films. To grow boron and nitrogen co-doped diamond films, 4 sccm $B(OCH_3)_3$ and 0-4.5 sccm urea were introduced into the chamber. These samples were designated as B4N0-B4N4.5 diamond films, respectively. A large negative bias (–100 V) was applied to Si-substrates in the nucleation stage to facilitate the formation of diamond nuclei on mirror smooth silicon surface. Moreover, –50 V bias voltages were applied to the substrates in the growth stage to maintain the diamond grains small. The diamonds were grown under this condition for about 1 h to reach a thickness about 1 μm.

The morphology and structure of the diamond films were examined using scanning electron microscopy (SEM, Joel) and Raman spectroscopies (Renishow), respectively. The electron field emission properties of the diamond films were measured using a parallel setup. The anode, indium tin coated glass was separated from the cathode, diamond films coated silicon, using 100 μm glass beads as spacer. The current-voltage (I-V) characteristics of the diamond films were measured by a Keithley 237 electrometers. The current-voltage (I-V) properties of the diamond films were analyzed by using the Fowler-Nordheim model. The turn-on field was defined by the intersection of the two straight line extrapolated from low-voltage and high voltage segments of the F-N plots. The effective work function ($\phi_e = \phi/\beta$), which is the ratio of true work function (ϕ) and field enhancement factor (β), of the diamond films can be deduced from the slope of the F-N plots.

To examine the local electron field emission properties of the diamond films, current image tunneling spectroscopic (CITS) technique in atomic force microscopy (AFM, Seiko SPA 500) was used. The AFM was set constant force mode such that the PtIr-coated Si-tip was maintained at a constant gap with respect to the diamond films. The 3 μm × 3 μm scanned area of the diamond films were divided into 64 × 64 segments. The bias voltage applied to the diamond films was swept in between ±3 V, while the PtIr(Si)-tip was staying at a segment for 50 ms. 64 × 64 tunneling current-voltage (I_t-V) curves were acquired, which were used to produce current image tunneling spectroscopies (CITS).

3. Results and Discussion

Typical microstructure and crystallinity of the boron-doped diamond films are shown as SEM micrographs and Raman spectroscopies in Figures 1 and 2, respectively. When the doping level is smaller than 3 sccm urea, these characteristics are insignificantly altered due to boron and nitrogen co-doping. However, electron field emission capacity of the diamond films increases from $(J_e)_{B4N0}$ = 50 μA/cm^2 to $(J_e)_{B4N15}$ = 200 μA/cm^2 under 22 V/μm applied field for lightly doped sample and abruptly increases to $(J_e)_{B4N3}$ = 1,500 μA/cm^2 for heavily doped films, which are illustrated as field emission characteristics in Figure 3. Fowler-Nordheim plots shown as inset in Figure 3 reveal that the turn-on field for B4N3 samples is around $(E_0)_{B4N3}$ = 6.4 V/μm, which is pronouncedly lower than that of the other diamond films. The effective work function (ϕ_e) for heavily doped samples (B4N3) is also significantly smaller than that of the lightly doped ones (B4N0 and B4N1.5).

Detailed examination on the micro- structure reveals that the grain size, which is uniformly distributed, decreases only slightly with urea content of the films. The grain size is about 0.7 μm for B4N0 samples and is about 0.6 μm for B4N3 samples. There exists some small grains, about 0.3 μm is size, among the large grains (Figure 1). Apparently, the difference in granular structure is not the prime factor resulting in such a pronounced change in field emission properties of the films.

Further increase in urea content to 4.5 sccm dramatically lowered the electron field emission capacity for the diamond films ($(J_e)_{B4N4.5}$ = 100 μA/cm^2) and pronouncedly increased the turn-on field ($(E_o)_{B4N4.5}$ = 9.2 V/μm), as shown in Figure 3. Raman spectroscopy in Figure 2 indicates the presence of G-band resonance peak, the signature of graphitic phase. SEM micrographs in Figure 1 reveal the marked change on films' morphology. The diamond grains aggregate, forming clusters about 1.5 μm in size, although the grains in the clusters are still very small, about 0.5 μm in size. These results imply that too high concentration of urea hinder the formation kinetics for the diamond nuclei. The degradation of the diamond quality is presumed to be the prime factor resulting in the dramatic reduction for the electron field emission properties of the over-doped diamond films.

To understand the true mechanism for altering the field emission characteristics of the diamond films, the localized electron emission behavior of the samples was investigated using

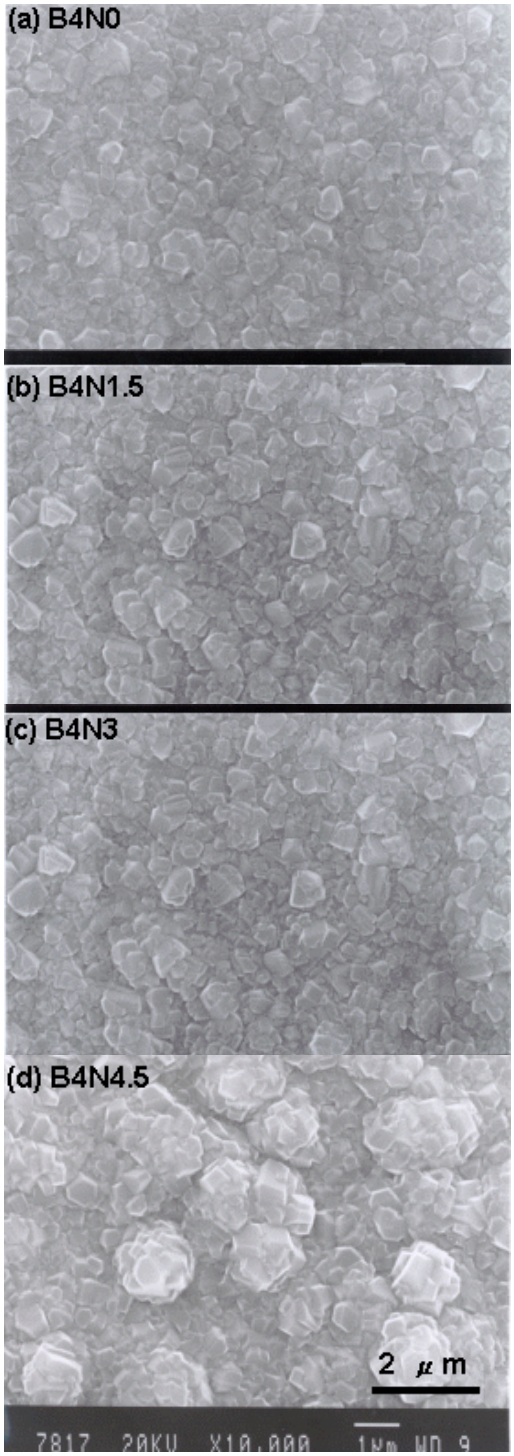

Figure 1. SEM micrograph of the diamond films co-doped with 3 sccm $B(OCH_3)_3$ and 0-4.5 sccm urea species

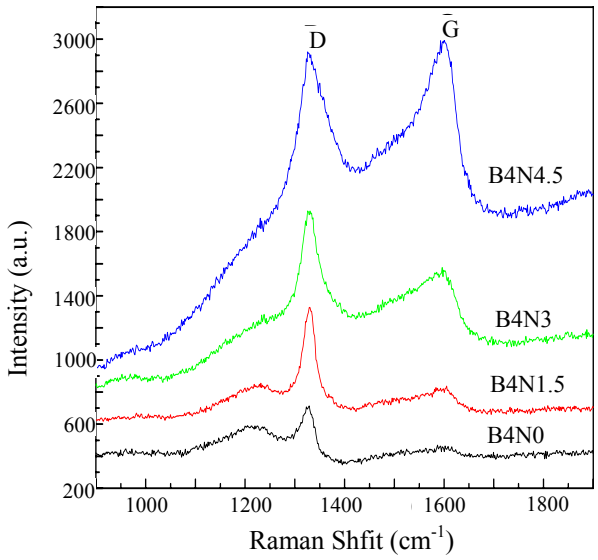

Figure 2. Raman spectra of the diamond films co-doped with 3 sccm $B(OCH_3)_3$ and 0-4.5 sccm urea species

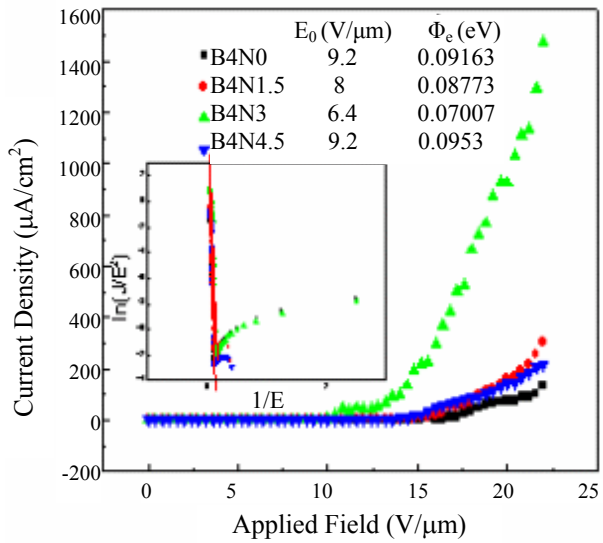

Figure 3. The electron field emission property of the diamond films co-doped with 3 sccm $B(OCH_3)_3$ and 0-4.5 sccm urea species (The inset shows the Fowler-Nordheim plots of the I-V curves.)

atomic force microscopies (AFM). Figure 4(a) shows one of the typical diamond grains in B4N3 samples, which is a pyramid about 500 nm in size, consisting of three (100)-type surfaces. To investigate the local field emission behavior of the films, the sample surface was divided into 64 × 64 segments and tunneling current-voltage (I_t-V) curves corresponding to each segment were acquired. Figure 5(a) illustrates the 3 typical I_t-V curves. It is surprising to observe that the I_t-V behavior is so much different between the surfaces.

Presumably, the positively biased tunneling current represents the tunneling of electrons from PtIr(Si)-tip to diamond surface and is proportional to the density of unoccupied (empty) states of the diamonds, whereas the negatively biased current corresponds to the tunneling of electrons from

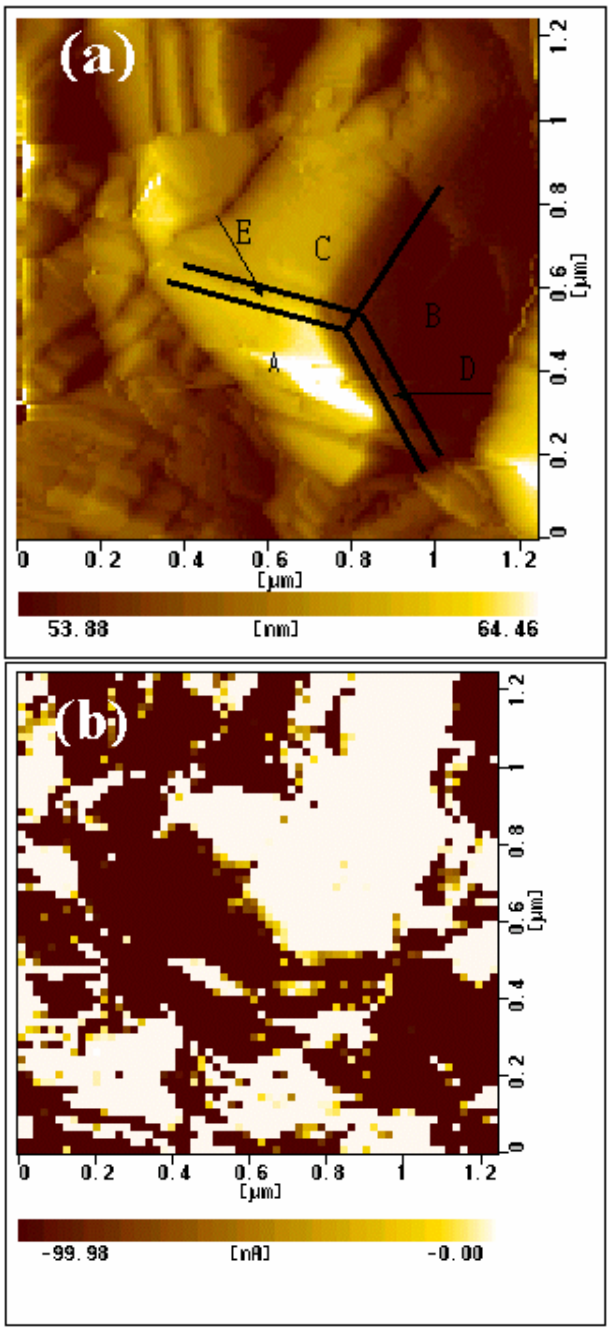

Figure 4. (a) AFM micrograph of a typical diamond grains with pyramidal geometry; (b) the current image tunneling spectroscopic (CITS) micrographs of the pyramidal grains with the diamond films biased at –3.0 V (The darker sports represent larger field emission current from diamond films to Pt Ir(Si)-tip.)

diamond surface to PtIr(Si)-tip and is proportional to the density of occupied states of the diamonds. The negatively biased current contains both the tunneling and field emitting electrons. Figures 4(a) and 5(a) infer that the surfaces $(100)_A$, and $(001)_C$ are conducting, while the surface $(010)_B$ is nonconducting. It is interesting to observe that the segments tunneling better also exhibit larger

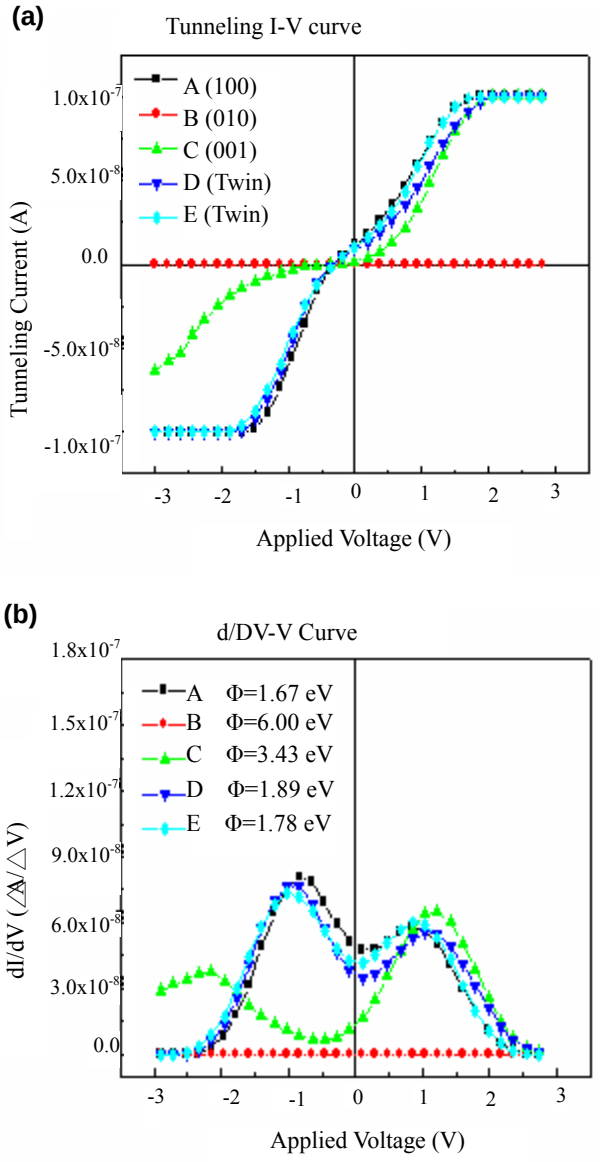

Figure 5. (a) The tunneling current-voltage (I_t-V) properties of the (100) surfaces of the pyramidal diamond grains and (b) the derivatives, dI_t/dV-V, of the tunneling current-voltage curves

field emitting capacity and vice versa. The derivatives of the I_t-V curves show the distribution of the density of states. Figure 5(b) indicates that surfaces $(100)_A$ and $(001)_C$ surface possess an empty states at around +0.8 eV and an occupied states at around –2.5 eV, resulting in an energy gap, which is in proportion to the energy barrier for electron emission, about $(E_g)_{A,C} = 3.3$ eV. In contrast, $(010)_B$ surface shows very wide energy gap. These results demonstrate clearly that the surface electronic properties are not uniform.

When the negatively-biased tunneling current (I_t) values of each segments is plotted for a given bias voltage, a current image tunneling spectroscopic

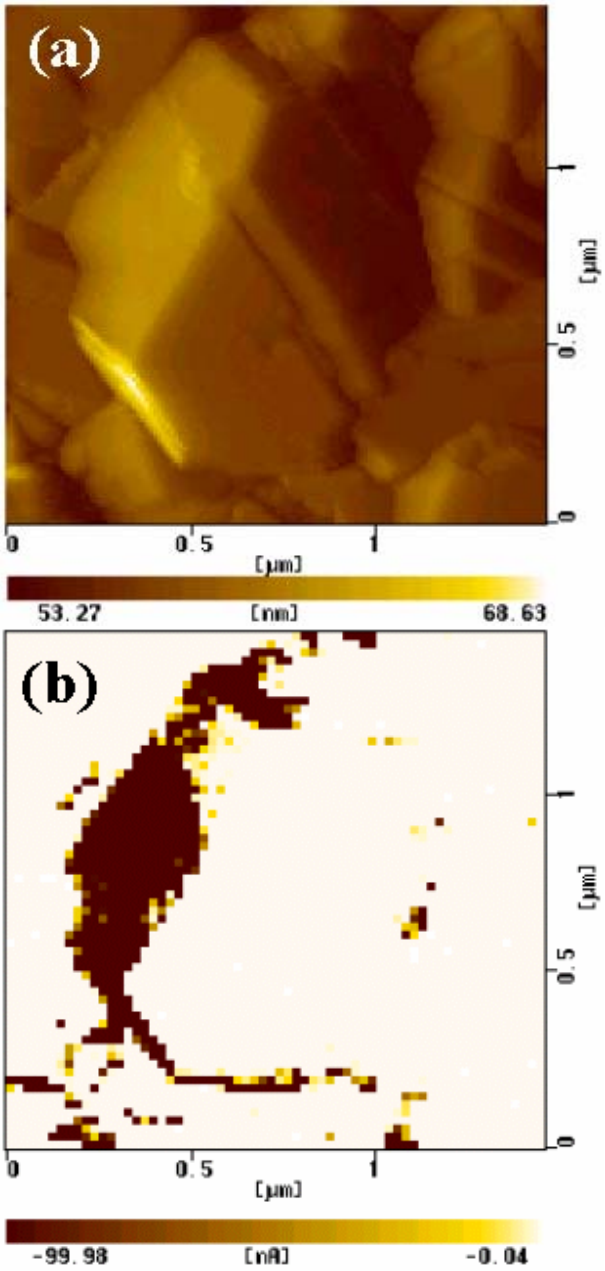

Figure 6. (a) AFM and (b) CITS micrographs for B4N1.5 nano-crystalline diamond films, which were doped with 4 sccm $B(OCH_3)_3$ and 1.5 sccm urea species (The darker spots represent the area emitting larger proportion of electrons.)

(CITS) map, representing the distribution of the tunneling/emission capacity of the diamond surface, is obtained. Figure 5(b) reveals the CITS maps of emission electrons, from diamond films to PtIr(Si)-tip, corresponding to V_{e2} = –3.0 V. The darker spots represent larger field emission current. In the area examined, only the $(100)_A$ and $(001)_C$ surfaces are emitting. Contrary to the common knowledge that the tip and edge of the samples emit more efficiently due to field concentration effect, Figure 4 and 5 imply that neither the tip the diamond pyramid nor the edges is emitting. Moreover, these figures show that the steps located at joining of $(100)_A$ and $(001)_C$ surfaces or at that of $(100)_A$ and $(010)_B$ surfaces exhibit significantly better local electron field emission properties than the flat surfaces. Such a phenomenon was observed for other samples, which are illustrated in Figures 6(a) and 6(b) for B4N1.5 grains. These results infer that the imperfect region is more emissive than the defect less area for the diamond grains.

Table 1. (a) The electron field emission characteristics (J_e and E_o)[a] of nano-crystalline diamond films co-doped with boron and nitrogen[b]; (b) local electron field emission behavior (η. and V_g)[c] of these diamond films examined using current image tanneling spectroscopic (CITS) technique

	B4N0	B4N1.5	B4N3	B4N4.5
(a) J_e ($\mu A/cm^2$)	50	200	1500	100
E_o (V/μm)	9.2	8	6.4	9.2
(b) η (%)	7.81	8.33	87.5	30.86
V_g (eV)	2.81	1.81	1.62	1.78

[a]Electron field emission characteristics: J_e = emission current density and E_o = turn-on field

[b]Diamond films B4N0, B4N1.5, B4N3, B4N4.5 were doped with 4 sccm $B(OCH_3)_3$ and 0-4.5 sccm urea.

[c]Local electron field emission behavior: η = emission ratio defined as the percentage of area emitting electron current density larger than 10 nA, when the films were biased at –3 V. V_g = voltage gap derived from the (dI/dV)-V curves of the tunneling current measured by CITS technique

The above results indicate that the I_t-V characteristics of the diamond films vary markedly among the regions on the samples. Local I_t-V curves measured by AFM represent the distribution of the regions possessing good electron field emission properties. Derivatives of the I_t-V curves, which represent qualitatively the distribution of density of states in the diamond films, provide the information of the energy gap (E_g). The energy gap qualitatively represents the energy barrier for electron to jump from valence band to conduction band for emitting. Similar measurements were performed for other boron and nitrogen co-doped samples and the results are shown in Table 1, revealing that the energy gap (E_g) decreases with urea content first up to B4N3 samples (E_g = 1.62 eV) and increases again for over-doped diamond films. Apparently, the reduction on energy gap (E_g)

due to boron and nitrogen co-doping can be ascribed to the induction of extra energy level (impurity states) in between the empty states (conduction band edge) and occupied states (valance band edge). How the boron and nitrogen species incorporated result in the formation of impurity states for the diamond films is not clear, as boron are known to act as donors with E_d = 0.2 eV and nitrogen in diamonds are known to behave as acceptors with E_a = 1.7 eV. The induction of carbonaceous vacancies is a possible cause, which, however, needs more detailed examination.

Similarly, CITS micrograph representing the distribution of tunneling current over the diamond films can be deduced by comparing the magnitude of tunneling current (I_t) at the same negative bias voltage, where the electrons were emitted from diamonds to the PtIr(Si)-tips. It should be noted that the tip-to-film distance was maintained at a same small value, while acquiring the tunneling current. No field concentration effect due to geometric factor of the emitting sites is expected. If we define the region possessing I_t-value larger than 10 nA as emitting area, the electron emission ratio, which is the percentage of the regions emitting, can then be deduced. Table 1 reveals that the B4N3 samples possess the largest emission ratio (η = 87.2%) among the B & N-doped (BnNm) diamond films, which, in conjunction with small energy gap ((E_g) = 1.62 eV), results in larger electron field emission capacity (J_e = 1,500 A/cm^2) for the samples.

4. Conclusion

Effect of boron and nitrogen co-doping on the electron field emission properties of the diamond films was examined using CITS (AFM). Tunneling current-voltage (I_t-V) characteristics measured by AFM indicate that incorporation of boron and nitrogen species induces the presence of impurity state. Such a characteristic is closely related to the local electron field emission behavior of the diamond films. The B4N3 samples possess the smallest energy gap (E_g = 1.62 eV) and, thereafter, can be turned on at the smallest electric field (E_o = 6.4 V/μm), exhibiting the largest field emission capacity (J_e = 1500 μA/cm^2). The emission ratio (η) of the same films is larger, as compared with other diamond films. Moreover, CITS measurement reveals that the tunneling properties of a single diamond grains vary with the surface of the grains.

Acknowledgments

The authors gratefully acknowledge the National Science Council, R.O.C. for the financial support through the project No. NSC-89-2112-M-007-080.

References

[1] Spindt, C. A.; Brodie, I.; Humphrey, L.; Westerberg, E. R. *J. Appl. Phys.* **1976**, *47*, 5248.
[2] Van Gorkom, G. G. P.; Hoeberechts, A. M. E. *J. Vac. Sci. Technol. B* **1986**, *4*, 108.
[3] Himpsel, F. J.; Knapp, J. A.; Van Vechten, J. A. *Phys. Rev.* **1979**, *20*, 624.
[4] Zhu, W.; Kochanski, G. P.; White, A. E. *Appl. Phys. Lett.* **1995**, *68*, 1157.
[5] Ku, T. K.; Chen, S. H.; Cheng, H. C. *IEEE Elec. Device Lett.* **1996**, *17*, 208.
[6] Glesener, J. W.; Morrish, A. A. *Appl. Phys. Lett.* **1996**, *69*, 785.
[7] Okano, K.; Koizumi, S.; Silva, SRP.; Amaratunga, G. *Nature* **1996**, *381*, 140.
[8] Okano, K.; Gleason, K. K. *Electronics Lett.* **1995**, *31*, 74.
[9] Geis, M. W.; Twichell, J. C.; Lyszczarz, T. M. *Appl. Phys. Lett.* **1996**, *68*, 2294.
[10] Hong, T. M.; Chen, S. H.; Chiou, Y. S.; Chen, C. F. *Appl. Phys. Lett.*, **1995**, *67*, 2149.
[11] W. Muller Cebert, Worcer, E.; Fuchs, F.; Wiland, C.; Koide, P. *Appl. Phys. Lett.* **1996**, *68*, 759.
[12] Won, J. H.; Hatta, A.; Yagyu, H.; Jiang, N.; More, Y.; Ito, T.; Sasaki, T.; Hiraki, A. *Appl. Phys. Lett.* **1996**, *68*, 2822.
[13] Chen, Y. H.; Hu, C. T.; Lin, I. N.; *J. Appl. Phys.* **1998**, *84*, 3890.
[14] Shih, C. F.; Liu, K. S.; Lin, I. N. *Diam. Rel. Mater.* **2000**, *9*, 1591.
[15] Vander Z. *Solid State Physical Electronics*; Prentice-Hall: Englewood Cliffs, NJ, U.S.A., **1968**, 144.

Manuscript Received: May 6, 2003
and Accepted: Jun. 10, 2003